Growth of oxygen-induced nanoscale-pyramidal facets on Rh(210) surface

Govind
Surface Physics and Nanostructures group, National Physical Laboratory, Dr. K.S. Krishnan Marg, New Delhi 110 012, India

Wenhua Chen, Hao Wang, and Theodore E. Madey
Department of Physics and Astronomy, Laboratory for Surface Modifications, Rutgers, The State University of New Jersey, 136 Frelinghuysen Road, Piscataway, New Jersey 08854, USA

(Received 8 October 2009; revised manuscript received 22 December 2009; published 9 February 2010)

Oxygen-induced nanometer scale faceting of the atomically rough Rh(210) surface has been studied using Auger electron spectroscopy, low energy electron diffraction (LEED), and scanning tunneling microscopy (STM). When the Rh(210) surface is annealed at temperature ≥ 550 K in oxygen (pressure $\geq 2\times 10^{-8}$ Torr), it becomes completely covered with nanometer-scale facets. LEED studies reveal that the faceted surface is characterized by three-sided nanoscale pyramids exposing one reconstructed (110) and two {731} faces on each pyramid. STM measurements confirm the LEED results and show that the average facet size ranges from 12 to 21nm when changing annealing temperature from 800 to 1600 K. Moreover, atomically resolved STM images show that the (110) face of faceted Rh(210) exhibits various reconstructions ($1\times n$, $n=2-4$) depending on oxygen coverage. Faceted Rh(210) is a potential template for studies of structure sensitive reactions.

DOI: 10.1103/PhysRevB.81.085415 PACS number(s): 68.55.J−, 68.55.A−, 68.37.Ef, 68.43.−h

I. INTRODUCTION

The morphological changes induced on solid surfaces by adsorbates have been a center of attraction for decades because of their wide applications in thin film growth, catalytic reactions and corrosion studies.[1] The interaction between adsorbates and substrates can enhance the anisotropy in surface free energy, which can lead to adsorbate-induced faceting of surfaces.[2] Faceting is a process whereby a clean metal surface covered with adsorbate and annealed at elevated temperatures undergoes morphological changes to reduce the total surface free energy. The faceted surface usually exposes faces that have more close-packed surface structures than the original planar surface, resulting in a reduced total surface free energy although the total surface area is increased. A suitable candidate for faceting studies is an atomically rough metal surface that has higher specific surface free energy than a close-packed surface of the same material and is less stable against the adsorbate-induced faceting.[3–15] The potential application of these faceted surfaces could be as model systems to study structure sensitivity and size effects in catalytic reactions[16–20] and as templates to grow metallic nanoclusters.[15,21]

Many studies have been performed on adsorbate-induced faceting of atomically rough surfaces, e.g., bcc W(111) (Refs. 8 and 9) and Mo(111),[6,8,10] fcc Rh(553),[13] Cu(210),[4,7] Ir(210),[11] Pt(210),[5] and Ni(210),[3,4] and hcp Re(12$\bar{3}$1) (Refs. 12 and 14) and Re(11$\bar{2}$1) (Ref. 15) surfaces. Recent studies on fcc (210) surfaces[3–5,7,11] indicate that facets can be induced due to the presence of different adsorbates, e.g., oxygen and active nitrogen can induce faceting of Cu(210) (Refs. 4 and 7) and Ni(210) (Refs. 3 and 4) while oxygen interaction or CO oxidation can provide favorable conditions to restructure the Pt(210) (Ref. 5) surface to form facets. Ir(210) (Ref. 11) shows the formation of pyramidal-type facets with {311} and (110) faces when annealed in oxygen at and above 600 K. The faceted Ir(210) surface has been used to study structure sensitivity and size effects in chemical reactions.[18–20]

In this work, we study morphological changes of Rh(210) induced by oxygen using low energy electron diffraction (LEED), Auger electron spectroscopy (AES), and scanning tunneling microscopy (STM), which is mainly motivated by the two considerations. First, Rh(210) has the same fcc structure as Ir(210), which enables us to compare with oxygen-induced faceting of Ir(210) leading to better understanding of the physical insight into the morphological changes in the facets with the nature of metal. We have previously found that oxygen can induce faceting of Ir(210) (Ref. 11) and faceted Ir(210) has been successfully used to explore structural and size effects in a series of important chemical reactions.[18–20] It is expected that faceted Rh(210) will be also used to probe for structure sensitivity and size effects in chemical reactions. Second, the study of Rh is of technological importance due to the fact that Rh is a catalyst component in current commercial three-way catalysts for reducing air pollution from automobile exhaust gases.[20] Rh(210) is an atomically rough surface and the unreconstructed Rh(210) surface has four layers of atoms exposed where the top layer atoms show C_{2v} symmetry (180° rotation with the [210] vector as the principal axis) as shown in Fig. 1. The Rh(210) surface also shows mirror reflection symmetry along (001) plane. Our results demonstrate that oxygen can induce faceting of Rh(210) and that the local geometric structure of the facets depends on the oxygen coverage. Our findings may have important implications for Rh-based catalysts operating under oxygen-rich conditions since the structures of the catalysts influence their catalytic performance.

II. EXPERIMENTAL DETAILS

The experiments were carried out in two different ultrahigh vacuum (UHV) chambers denoted as LEED and STM chambers, respectively. All LEED images shown in this pa-

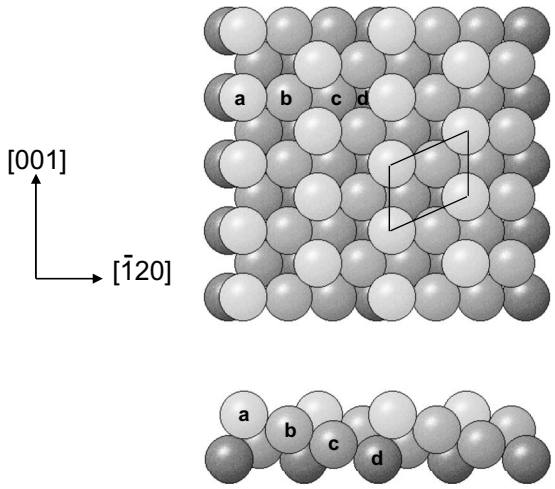

FIG. 1. Hard-ball model of Rh(210) surface (top and side view) showing four exposed layers.

per were obtained in the LEED chamber that also contains a quadrupole mass spectrometer for residual gas analysis and an AES instrument for checking the cleanness of the Rh surfaces. All the STM experiments described here were performed in the STM chamber at room temperature using a hybrid variable temperature Omicron STM with tungsten tips. The instrument is housed in a home-built UHV system equipped also with reverse view LEED and AES.

The same Rh(210) crystal was used in both chambers. The sample was cut from a single crystal Rh (99.99%) rod, ~10 mm in diameter, ~1.5-mm thick, aligned within 0.5° of the (210) orientation and polished to a mirror finish. In the LEED chamber, the sample was supported by two rhenium leads (approximately $12\times3\times0.1$ mm^3) that were spot-welded directly to the rear of the sample (rhenium has a very high melting point ~3459 K and has no low melting point alloys with rhodium[22]). The same leads were used for resistive heating where a high current (up to 30 A) can be passed through the leads and sample to achieve sample temperatures up to 1300 K. For accurate temperature measurement a *C*-type (W–5%Re/W–26%Re) thermocouple was spot-welded directly to the rear of the sample. The sample support assembly also included a tungsten filament for e-beam heating; a temperature up to 2000 K can be achieved by flashing the sample. The sample was cleaned by repeated cycles of Argon sputtering (1 keV, 3.5 μA) at 300–650 K [initially at 300 K and then at increasingly higher temperature ($<$650 K)], annealing in O_2 (2×10^{-8} Torr) at 1000–1200 K followed by rapid flashes to ~1600 K in UHV to remove oxygen from the surface. In the STM chamber, the sample was mounted on a redesigned Omicron tantalum sample plate, which was described elsewhere,[23] to allow for e-beam heating up to 2000 K. The sample temperature was measured by a pyrometer. The sample preparation for STM measurements was performed with the similar procedures described above. The faceted O/Rh(210) surface was confirmed by LEED prior to the STM measurements. The oxygen dosing was achieved by back filling the chamber using research purity O_2. All exposures are reported in Langmuir (1 L $=10^{-6}$ Torr s) and are uncorrected for ion gauge sensitivity.

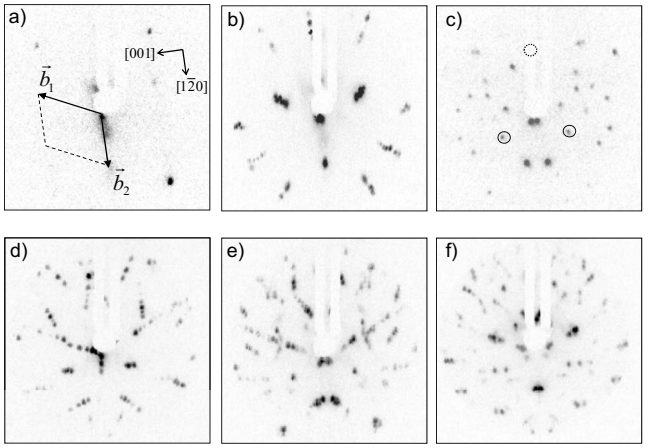

FIG. 2. LEED patterns from planar and faceted Rh(210) surfaces at different incident electron-beam energy (E_e): planar surface at (a) $E_e=60$ eV, (b) $E_e=20-110$ eV; faceted O/Rh(210) surface at (c) $E_e=60$ eV, (d) $E_e=20-50$ eV, (e) $E_e=56-84$ eV, and (f) $E_e=90-120$ eV. The primitive unit cell of the LEED pattern in (a) is labeled together with its main symmetry directions in real space.

III. RESULTS

A. LEED Study

Figure 2(a) shows a LEED pattern from a clean Rh(210) surface; all the spots are characteristics of the unreconstructed (1×1) structure. When the incident electron-beam energy (E_e) increases, all the diffraction spots move and converge to the center of the LEED screen as shown in Fig. 2(b), which indicates that the surface is planar. No additional feature is observed in the LEED pattern after oxygen exposure up to 100L at room temperature on the clean Rh(210) surface except that the background signal intensity increases after the oxygen exposure. The increase in the background signal may be attributed to additional diffuse scattering from the oxygen overlayer or the random adsorption of oxygen atoms on available sites on Rh(210).

Figures 2(c)–2(f) shows the LEED pattern of the Rh(210) surface predosed with 10 L oxygen followed by annealing in O_2 (2×10^{-8} Torr) at 850 K for 2 min and cooling to room temperature in O_2. When the electron-beam energy (E_e) increases, all the diffraction spots converge, respectively, to one of the three distinct points labeled by circles in Fig. 2(c). These three points are specular reflections from three different surface planes that are tilted with respect to the planar Rh(210) surface and the complete LEED pattern from the faceted surface is a superposition of three sets of LEED patterns that originate from three tilted surface planes. The emergence of these patterns can be interpreted as the formation of three sided nanopyramidal facets on the Rh(210) substrate surface. In previous studies on W(111) (Ref. 24) (covered with metallic overlayers) and Ir(210) (Ref. 11) (covered with oxygen) existence of three specular diffraction spots is also observed which reflects the formation of three sided pyramids. However, in these studies the specular spot positions and the corresponding facet tilt angles are different from those of present study as described below.

Figure 3 shows the evolution of diffraction spots of the faceted surface with annealing temperature obtained by an-

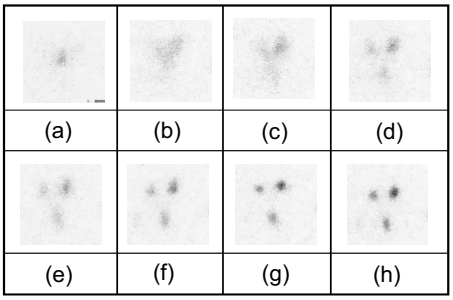

FIG. 3. Evolution of the LEED spots from faceted O/Rh(210) surface with annealing temperature (a) 400 K, (b) 450 K, (c) 500 K, (d) 550 K, (e) 600 K, (f) 650 K, (g) 750 K, and (h) 850 K at incident electron-beam energy 74 eV. The LEED spot in (a) corresponds to the $(-1,-1)$ beam from the planar O/Rh(210) surface based on the notation in Fig. 2(a).

nealing 10 L oxygen-predosed Rh(210) in O_2 (2×10^{-8} Torr) for 2 min, where a part of each pattern has been magnified. From 400 to 500 K the (1×1) diffraction beams from the planar surface become progressively fainter and three additional beams from the faceted surface emerge and become sharper gradually. With increasing the annealing temperature to 550 K, the diffraction beams corresponding to the planar surface completely disappear and the three beams corresponding to the faceted surface become well-separated spots. On increasing the annealing temperature from 550 to 850 K, LEED spots do not show any change in their positions but the change in the spot size can be observed [Figs. 3(d)–3(h)], i.e., diffraction spots become sharper as annealing temperature increases. In addition, it is also observed that the diffraction spots corresponding to faceted O/Rh(210) surface are stable in UHV up to 900 K. On further increasing the sample temperature (>900 K) the diffraction beams of the faceted surface disappear and the faceted surface reverts to the original (1×1) planar surface.

The orientations of the three facets are determined by comparing the positions of the specular beams of the facets with the LEED spots from the planar (210) surface.[12] The positions of the specular beams corresponding to three facet planes are marked as A, B, and C in the LEED pattern shown in Fig. 4(a). The specular beams A and B show a mirror reflection symmetry around the (001) plane. Comparison of the LEED pattern from the faceted surface with those from

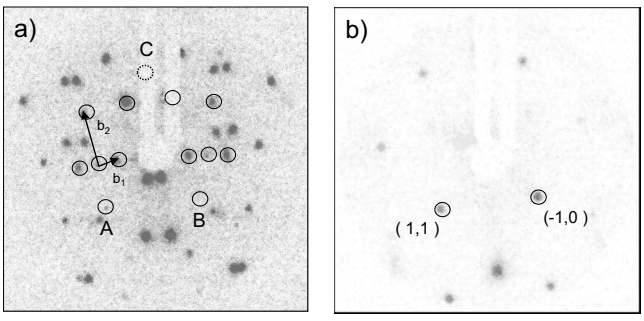

FIG. 4. (a) LEED pattern from the faceted surface at incident electron-beam energy E_e=70 eV and (b) LEED pattern from the planar surface at incident electron-beam energy 160 eV.

the planar surface at different electron beam energies reveals that the positions of the specular beams A and B from the faceted surface are located almost in the same positions on the LEED screen as those corresponding to (1,1) and $(-1,0)$ diffraction spots from the planar (210) surface at electron beam energy 160 ± 5 eV shown in Fig. 4(b). The spatial orientations of the (1,1) and $(-1,0)$ beams can be determined from the structure of reciprocal rods of Rh(210) and the Ewald sphere construction.[25] We first calculate the angle between a facet plane corresponding to the specular beam B and the (210) plane. The calculated angle between the $(-1,0)$ beam and the normal direction of (210) is $16.2\pm0.2°$; therefore the tilt angle of the facet defined by specular beam B relative to the (210) plane is $8.1\pm0.1°$. Due to the symmetry, the tilt angle between the other facet plane A and the (210) plane is also $8.1\pm0.1°$. The azimuthal angle between these two faceted planes was also measured and found to be $\Phi=132\pm4°$. Based on the tilt angles between the faceted planes and the (210) plane as well as azimuthal angle between the two symmetric facets, the Miller indices of these two facets are identified as (731) and $(73\bar{1})$ planes. The tilt angle between the third facet, defined by the specular beam C in Fig. 4(a), and the (210) plane is also calculated in similar way. However, from Fig. 4(a), the exact position of the specular beam C is difficult to observe as the specular beam corresponding to this facet is blocked by the leads of the sample support assembly. In this case the position of the specular beam C can be determined by extrapolating the motion of the diffraction spots corresponding to the facet with changing the electron-beam energy (E_e). The estimated tilt angle between the facet and the (210) plane is $18\pm2°$. The closest choice for the facet orientation corresponding to specular beam C is the (110) plane, and the theoretical tilt angle between the (210) plane and (110) plane is 18.43°. It is also observed that the diffraction spots from (110) facet contain some weak diffraction spots in the rectangular lattice and the positions of these spots are defined by vectors $\vec{b}_1$ and $\vec{b}_2$ in Fig. 4(a). The ratio between two vectors ($|\vec{b}_1|/|\vec{b}_2|$) is ~2.6, which suggests that the LEED pattern from the (110) plane is better described by a (110) (1×2) reconstructed LEED pattern. The identification of the three facets above are supported by the ideal tilt angles between the facets and the (210) plane calculated from the well-known geometric properties of cubic crystals, which are $\theta_{731}=8.4°$, $\theta_{110}=18.43°$, and $\phi_{731}=132°$ (azimuthal angle between the (731) and $(73\bar{1})$ plane).

B. STM study

Figure 5(a) shows an STM image of a faceted Rh(210) surface prepared by predosing of 10 L oxygen at 300 K followed by annealing in O_2 at 850 K for 2 min and then cooling to 300 K in presence of oxygen (4×10^{-8} Torr). The faceted Rh(210) surface is fully covered by well-defined three-sided nanopyramids with similar shape, which implies that the pyramids expose faces of identical crystallographic orientations. To reveal the atomic details, we differentiate the height of STM image along x direction (x slope); with this

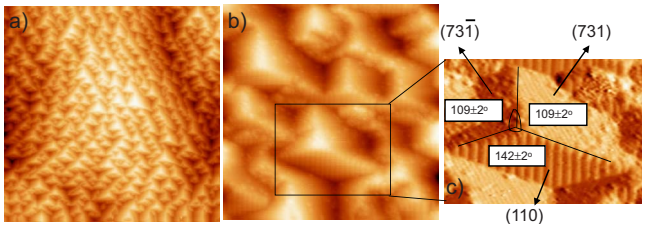

FIG. 5. (Color online) STM images of a fully faceted O/Rh(210) surface prepared by predosing 10 L oxygen followed by annealing in O_2 (4×10^{-8} Torr) at 850 K for 2 min and then cooling in oxygen to room temperature. Scan parameters are: (a) 3000 $\times$3000 Å^2 (V=2 V and I=1 nA), (b) 500$\times$500 Å^2 after the X slope taken (V=2 V and I=1 nA), and (c) 250$\times$220 Å^2 after the X slope taken (V=1 V and I=0.5 nA). The azimuthal angles of edge lines between different facets are also shown.

procedure the details of STM image can be enhanced at the cost of losing height information. In Fig. 5(b), an x-slope image of faceted Rh(210) surface has been shown with the orientations of the facets, i.e., {731} (upper-left and upper-right pyramid sides) and (110) (bottom pyramid side). The orientations of the facets identified by LEED can be further confirmed by measuring azimuthal angles between the edge lines of the facets as shown in Fig. 5(c). The average facet size ($\langle l\rangle$) of these nanopyramids can be estimated via the average pyramid number density $\langle n\rangle$ as $\langle l\rangle=\langle n\rangle^{-1/2}$, i.e., inverse of square root of total number of pyramids per unit area.[18,26] To determine the average pyramid size $\langle l\rangle$, we consider distinct pyramids that do not significantly deviate from the typical range in size or distance from neighboring pyramids. The calculated average pyramid size for the above surface is found to be $\langle l\rangle_{850\ \mathrm{K}}\sim18$ nm. However, we have found that the average pyramid size varies from 12 to 21 nm (images not shown), depending upon the annealing temperature, i.e., the higher the annealing temperature the bigger the average facet size. The biggest average nanopyramid size can be obtained by flashing the Rh(210) surface in oxygen (1×10^{-7} Torr) to 1600 K.

Figure 6 shows STM image of the (731) plane and corresponding cross-section profiles of the lines. The measured distance between the atomic rows along line 1 is 5.6$\pm$0.2 Å while the measured distance between the atomic rows along line 2 is 4.3$\pm$0.2 Å. A comparison between the calculated[27] and measured distances between atomic rows on (731) plane is shown in Table I, where vectors **a** and **b** are the unit cell vectors of (731) plane. Although (731) plane is rougher than (210), it is a vicinal (100) surface with kinked steps, which may account for the apparent stability of the {731} facets upon adsorption of oxygen. The analysis of the STM images confirms that the surface structure of the {731} facets of the pyramids remains the same for different oxygen coverages studied, however the (110) facet of the pyramids show significant structural changes with oxygen coverage.

The STM images for coverage-dependent structural changes in (110) facet obtained by annealing 10 L oxygen predosed Rh(210) in O_2 ($R\times10^{-8}$ Torr, R=2,3,4) for 2 min at 850 K are shown in Figs. 7(a)–7(c) and corresponding cross-section profiles of the lines along [001] direction are presented in Figs. 7(d)–7(f). The measured spacing between adjacent atomic rows of the (110) facet along the [001] direction is 7.9$\pm$0.2 Å for R=2 while it is 11.4$\pm$0.2 Å, and 15.6$\pm$0.2 Å for R=3 and R=4, respectively. The atomic distance between Rh-Rh atoms along [001] direction in Figs. 7(d)–7(f) is approximately two, three, and four times of that of an unreconstructed (110) plane (3.80 Å). The measured nearest-neighbor (nn) distance along [1$\bar{1}$0] direction is found to be 2.6$\pm$0.2 Å for all these surfaces, which compares reasonably with the atomic distance in this direction (2.7 Å) for an unreconstructed (110) surface. The error bar between the measured values and the calculated values may be attributed to instrumental factors such as thermal drift and piezoelectric creep. The corrugation measured along [001] for all these structures is found to be 0.5$\pm$0.15 Å while it is 0.1$\pm$0.02 Å in the protruding row observed from the line scan presented in Figs. 7(d)–7(f). These values are summarized in Table I.

Previous STM studies of oxygen on Rh(110) by Murray *et al.*[28] and Leibsle *et al.*[29] demonstrated that the oxygen can induce various reconstructions on the Rh(110) surface depending upon the oxygen coverage. These studies showed ($1\times n$) missing row reconstruction of Rh atoms where every second, third, fourth, and fifth atomic Rh row is missing along the [1$\bar{1}$0] direction depending upon the oxygen coverage. The oxygen atoms adsorbed in the zigzag fashion in troughs along the [1$\bar{1}$0] direction occupy threefold coordination sites, which gives rise to a variety of structures (2

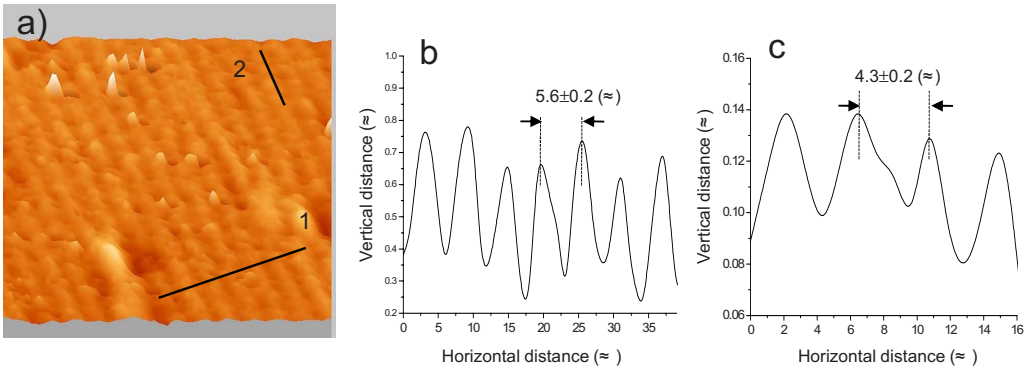

FIG. 6. (Color online) (a) STM image of (731) facet of faceted O/Rh(210) (104$\times$84 Å^2) (V=1.2 V and I=0.5 nA). (b) Cross-section profile of line 1. (c) Cross-section profile of line 2.

TABLE I. Experimentally measured and theoretically calculated characteristic distances and tilt angles of different facets with respect to (210).

Facet	θ_{exp} (deg)	θ_{th} (deg)	Row-to-row$_{exp}$ along $\vec{a}$ (Å)	Row-to-row$_{th}$ along $\vec{a}$ (Å)	Row-to-row$_{exp}$ along $\vec{b}$ (Å)	Row-to-row$_{th}$ along $\vec{b}$ (Å)
{731}	8.1 ± 0.5	8.4	5.6 ± 0.2	6.01	4.3 ± 0.2	4.66

Facet	θ_{exp} (deg)	θ_{th} (deg)	Row-to-row$_{exp}$ along [001](Å)	Row-to-row$_{th}$ along [001](Å)	nn$_{exp}$ along $[1\bar{1}0]$ (Å)	nn$_{th}$ along $[1\bar{1}0]$ (Å)
(110)(1×2)	18 ± 2	18.43	7.9 ± 0.2	7.61	2.6 ± 0.2	2.7
(110)(1×3)			11.4 ± 0.2	11.41		
(110)(1×4)			15.6 ± 0.2	15.21		

$\times 2)p2mg$, $c(2\times 6)$, $c(2\times 8)$, and $c(2\times 10)$ depending upon the oxygen coverage at annealing temperature 700 K. A corrugation of 0.7 Å in the missing rows and 0.16 Å in the protruding rows are observed.[28] Furthermore, it is observed that on Rh(110) these $c(2\times 2n)$ surface reconstruction can be transformed to (110) $(1\times n)$ reconstruction using hydrogen interaction at room temperature.[30] In view of these results, we interpret the observed parallel stripes on (110) faces on faceted Rh(210) as (110) terraces which exhibit every second, third, and fourth close-packed Rh missing row along $[1\bar{1}0]$ direction and show (1×2), (1×3), and (1×4) reconstruction of Rh atoms for different oxygen coverage.

Based on our LEED and STM measurements, a schematic of a single pyramid on faceted Rh(210) is presented in Fig. 8(a). Figure 8(b) shows the ball model of the fcc (731) surface and Fig. 8(c) shows (110) surface with a variety of $(1\times n)$ reconstruction, where every alternate nth atomic rows oriented in $[1\bar{1}0]$ direction are removed from the top layer and subsequently atomic rows from second and third layers are exposed to the vacuum. It should be noted that Fig. 8 illustrates structural models of the clean (731) and reconstructed (110) planes, where adsorbed oxygen atoms are not drawn. In fact, when oxygen from oxygen-covered faceted Rh(210) was removed by reaction with H_2,[18] the LEED pattern on the faceted surface did not change but with reduced background intensity (image not shown), indicating that oxygen adsorbs randomly on the Rh facets with (1×1) structures and thus did not induce extra LEED spots.

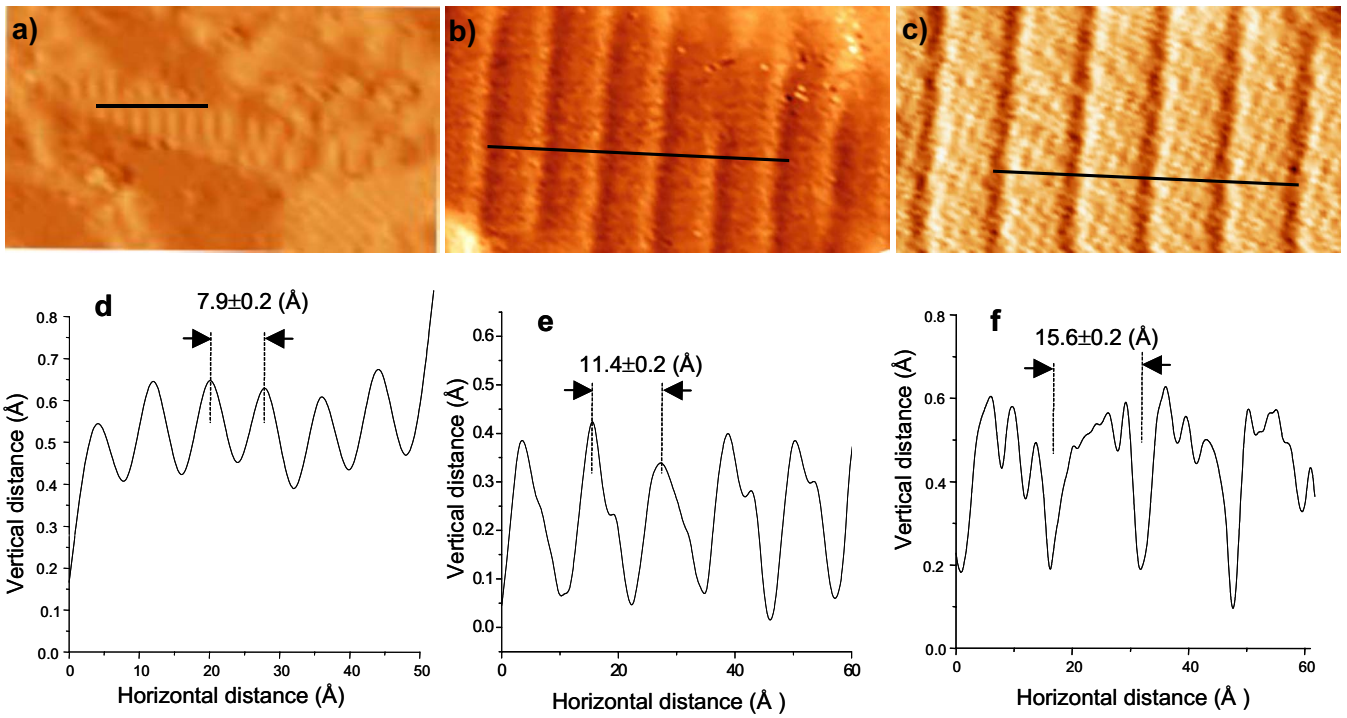

FIG. 7. (Color online) STM images of the (110) facet from faceted O/Rh(210) prepared by predoing 10 L oxygen followed by annealing in oxygen at 850 K for 2 min and then cooling to room temperature in oxygen. Oxygen pressures are: (a) 2×10^{-8} Torr, (b) 4×10^{-8} Torr, and (c) 6×10^{-8} Torr. The sizes of the images are (a) 250×250 Å^2, (b) 105×85 Å^2, and (c) 94×50 Å^2 ($V=1.2$ V and $I=0.5$ nA). The cross-section profiles of the lines along [001] in images (a)–(c) are represented in (d)–(f).

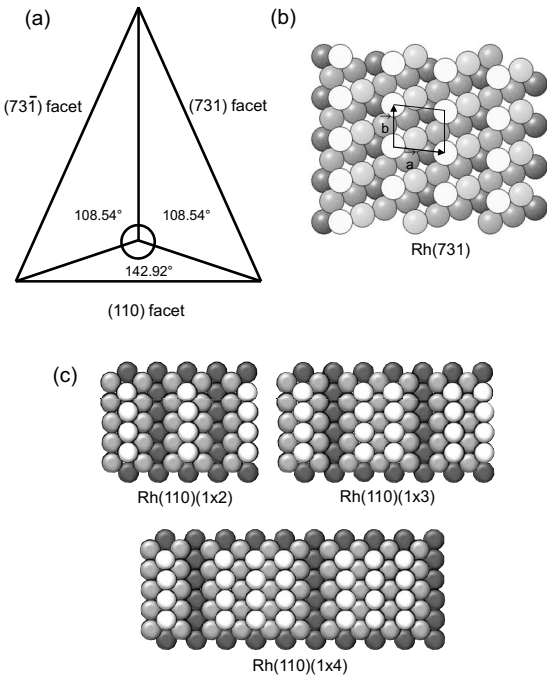

FIG. 8. (a) Schematic of single pyramid from the faceted Rh(210) surface. (b) Hard-ball model of Rh(731) surface and (c) Hall-ball models of Rh(110)$(1\times n)(n=2,3,4)$ surfaces.

IV. DISCUSSION

Surface faceting can be understood as a morphology change from a planar surface to a hill-and-valley structure driven by thermodynamics (anisotropy in surface free energy) and controlled by kinetic factors such as nucleation and diffusion.[1] The thermodynamics of these facets is usually understood in the context of equilibrium crystal shape (ECS); when facets are formed on planar surface, all the thermally stable facets must be present in the ECS.[31] For a clean metal surface, the anisotropy of the surface free energy is generally so small that a thermally annealed surface with relatively high surface free energy [e.g., W(111),[8] Ir(210),[11] and Re(12$\bar{3}$1) (Refs. 12 and 14)] can still retain its original orientation against faceting. However, when the planar surface is covered by a thin layer of adsorbate atoms, the surface free energy decreases due to the energy release from the formation of chemical bonds on the surface and in addition the anisotropy of surface free energy also changes. The change in the anisotropy of the surface free energy depends on several factors such as the binding energy of the adsorbate to the substrate bond, the geometry of the bond, and the coverage of the adsorbate molecules, which is also important for the determination of the morphology of the faceted surface. When the size of the facets is large enough such that the overall contribution of the step edges, kinks, and strain to the formation energy is rather small, the energetic requirement for facet formation can be expressed as[32]

$$\sum_f \gamma_f A_f - \gamma_p A_p < 0, \tag{1}$$

where γ_f (γ_p) is the specific surface free energy of the "$f(p)$" faceted surface (planar surface) per unit area and A_f (A_p) is the total surface area of the faceted (planar) surface. Since in the present case three facets are formed on the initially planar surface after adsorption of oxygen, the above equation converts into the following condition, which has to be fulfilled in order to show facet formation:

$$\sum_f \frac{\lambda_f}{\cos\,\theta_f} \cdot \gamma_f - \gamma_p < 0, \tag{2}$$

where θ_f is the tilt angle between facet "f" and the (210) plane, and λ_f is the structural coefficient describing the partial contribution of facet f to the total projected area on (210) plane. In the case of a fully faceted surface, λ_f is proportional to the surface area covered by face f such that sum of λ_f, i.e., $\Sigma_f \lambda_f$ equal to 1. From Eq. (2), the facet formation is possible only when sum of the surface energy of the facets is less than the planar surface energy. In the present study, oxygen induces faceting of Rh(210) which exhibits {731} and (110) faces on Rh(210) surface, the Eq. (2) can be read as

$$\frac{\lambda_{731}}{\cos\,\theta_{731}}\gamma_{731} + \frac{\lambda_{73\bar{1}}}{\cos\,\theta_{73\bar{1}}}\gamma_{73\bar{1}} + \frac{\lambda_{110}}{\cos\,\theta_{110}}\gamma_{110} < \gamma_{210}. \tag{3}$$

The surface free energy (γ) of the system, surface excess energy per unit area of a particular facet, can be obtained from surface electronic-structure calculations.[33–37] However, for clean metal surfaces with bulk truncated structures, a qualitative comparison of γ can be achieved by simply counting the numbers of broken bonds when the crystal is cleaved (in a thought experiment) to form a surface. It is important to mention here that in a bulk truncated configuration, the surface is defined as a slab in which the nn's of all atoms are fewer than those in the bulk. For fcc (210), the atoms in the topmost layer have 6 and 9 nn's in the second layer and 11nn's in the third layer. From the fourth layer downwards, the number remains the bulk value of 12. In other words, fcc (210) has a nn sequence of (6, 9, 11, 12). The nn sequence of fcc{731} and (110) are (6,7,9,10,11,12) and (7,11,12), respectively. To a first approximation, we consider only the nn bonds on clean Rh surfaces based on the broken bond counting method so the surface energies of (210), {731}, and (110) surfaces can be calculated. The surface energies of clean planar and faceted surfaces and the corresponding structural coefficients (λ_f) are summarized in Table II. If we assume all the involved surfaces are clean and substitute their surface energy values in Eq. (3), the clean Rh(210) surface does not transform spontaneously to pyramids with {731} and (110) facets due to no energy gain for such a transformation. This agrees well with the experimental observation that the clean Rh(210) surface is thermally stable. However, upon annealing Rh(210) in O_2 at elevated temperature ($\geq$550 K), {731} and (110) facets form on the Rh(210) surface. This indicates that adsorption of oxygen can induce an anisotropic change in the surface free energies of (210), {731}, and (110). The observation of {731} facets is also supported by early LEED study performed by Tucker[38] on Rh(210) surface. However, Tucker observed diffraction spots corresponding to only {731} facets on Rh(210) when annealing the surface in an oxygen background of 1×10^{-7} Torr at 573 K. Unfortunately, Tucker's conclusion

TABLE II. The specific surface energies (γf) of the (210), {731}, and (110) planes when they are clean in the units of broken bond number per unit surface area, where a is the size of the cubic cell of Rh. The numerical ratios of specific surface energies between the facets and (210) plane are in the third column. The tilt angles of the facets with respect to (210) are in the fourth column. The last column shows the structure coefficient (λf) of the facets in the simplest case: the planar (210) surface is completely covered by {731} and (110) facets.

Surface	γf	$\frac{\gamma_f}{\gamma_{210}}$	$\cos\theta_f$	θ_f (degree)	$\frac{\gamma_f}{\gamma_{210}\cos\theta_f}$	λ_f
(210)	$\frac{4\sqrt{5}}{a^2}$	1	1	0	1	1
{731}	$\frac{68}{\sqrt{59}a^2}$	$\frac{17}{\sqrt{295}}=0.990$	$\frac{17}{\sqrt{295}}$	8.2	1	0.425
$\{73\bar{1}\}$	$\frac{68}{\sqrt{59}a^2}$	$\frac{17}{\sqrt{295}}=0.990$	$\frac{17}{\sqrt{295}}$	8.2	1	0.425
(110)	$\frac{6\sqrt{2}}{a^2}$	$\frac{3}{\sqrt{10}}=0.949$	$\frac{3}{\sqrt{10}}$	18.4	1	0.15

does not appear to consider the fact that {731} facets cannot maintain the overall orientation of the initial planar Rh(210) surface. It is most likely that the specular spot corresponding to (110) facet was outside the LEED screen[15] in Tucker's experiment. In addition, Tucker has found that the diffraction spots are completely replaced by those corresponding to (100) and (110) planes when annealing in oxygen pressure 1×10^{-6} Torr at the same temperature. STM confirmation of this morphological evolution under high oxygen pressure (1×10^{-6} Torr) is necessary and will be the subject of future study.

The oxygen-induced enhancement of surface energy anisotropy has also been observed in a number of other systems. The planar Ir(210) surface transforms by pyramidal faceting with {311} and (110) facets[11] while oxygen interaction induces faceting on Cu(115). In the latter case, the change in the surface-energy anisotropy causes the Cu(115) surface converts to (104) and (014) facets that form spontaneously together with stepped facets whose orientation gradually change from (115) to (113) as the (014) facets grow.[39] Previous studies[33,40] suggest that enhancement in the anisotropy of surface free energy or reduction in surface free energy is caused by oxygen adsorption on preferential sites on the facets, which depends upon oxygen coverage and the O-metal binding energy on different facets. A qualitative explanation of faceting or the coverage-dependent evolution of surface morphology can be given by considering that the area-weighted combinations of all the facets and steps together with the energy requirement [Eq. (1)] must have lower surface free energy than the original planar surface.

Besides surface faceting, we have also observed reconstruction of the (110) facet depending upon the oxygen coverage. The oxygen-induced reconstruction on the (110) facet of faceted Rh(210) as a function of coverage is a clear illustration of the interplay between adsorbate-adsorbate, adsorbate-substrate, and substrate-substrate interactions. The structure of the metal surface changes with oxygen coverage, which minimizes the surface free energy. The energetics of the various reconstructions observed on (110) facet of faceted Rh(210) can be understood as the restructuring of surface Rh atoms in order to maximize the bonding and stability of the adsorbate-substrate complex. The reconstruction is driven by thermodynamics and occurs when stronger adsorbate-substrate bonds that form compensate for a weakening of bonds between substrate atoms, an inevitable accompaniment to the chemisorption of O-induced restructuring process. The oxygen-induced reconstruction on planar Rh(110) surface has already been observed in STM (Refs. 28–30, 41, and 42) and confirmed by LEED I-V analysis,[43] which suggests that the clean Rh(110)-(1×1) surface lowers its free energy by relaxations of the interlayer spacing. With the adsorption of more than 0.5 geometric monolayer (ML) oxygen at elevated temperatures, the metal surface reconstructs into the Rh(110)-$(1\times n)$ missing-row structure. This structure has oxygen adsorbed on top of the ridges of the $(1\times n)$ missing-row structure in fcc threefold hollow sites. These reconstructed surfaces are found to be stable due to the formation of more (111)-type microfacets and the capping of the lowest coordination Rh atoms at the surface layer by chemisorbed oxygen. Unlike oxygen-induced reconstruction observed on other fcc metals such as Ag(110),[44] Ni(110),[45] and Cu(110),[46,47] which appears to be driven by the formation of chains of alternating metal and oxygen atoms along [001] direction, the reconstruction of the Rh(110) facet is driven by the formation of missing rows along the $[1\bar{1}0]$ direction; a similar case can be found in oxygen-induced reconstruction of Pd(110).[48]

The theoretical studies on Rh surfaces[49–51] suggest that in the clean-state missing row reconstructions cannot be formed naturally as additional energy is required to reconstruct the surface Rh atoms. The reconstruction on the Rh(110) surface has been studied as the relaxation of Rh atoms in different layers due to the stress formation. Using density functional theory Stokbro and Baroni[52] have calculated the oxygen chemisorption energy for oxygen on the unreconstructed and (1×2) reconstructed Rh(110) surfaces. The calculated chemisorption energy for 0.5 ML O on reconstructed Rh(110)(1×2) surface is found to be larger than that on unreconstructed Rh(110) (1×1) surface. In addition, these studies show that the oxygen-induced reconstructed surface reverts back to unreconstructed surface at 1 ML O. However, we did not observe such feature in the present study as the reconstructed (110) face of faceted Rh(210) surface remains reconstructed for all oxygen pressure up to 1×10^{-6} Torr.

Theoretical calculations for oxygen on faceted Rh(210) are necessary to give an explanation.

V. CONCLUSION

In the present work, we focus on the adsorbate-induced modification of the surface free energy that brings a change in the surface morphology of the substrate. We have observed an oxygen-induced pyramidal faceting of Rh(210) surface with two {731} faces and one reconstructed (110) face on each pyramid when annealing Rh(210) in O_2 at and above 550 K. The average pyramid size ranges from 12 to 21nm, which can be controlled by changing the annealing temperature from 800 to 1600 K in O_2. As the oxygen coverage changes, the surface structure of the {731} facet remains the same while that of (110) facet shows $(1\times n)$ missing row reconstructions. The faceted surface reverts to the planar surface when annealing in UHV for temperatures >900 K. Theoretical studies are necessary to give detailed energetic descriptions of the bonding characteristics between oxygen and Rh on different facets and the change in the surface energy anisotropy. The faceted Rh surfaces provide possible model systems to study structure sensitivity in Rh-based catalytic reactions as well as potential nanotemplate to grow nanoclusters.

ACKNOWLEDGMENTS

Discussions with Q. Shen and R. A. Bartynski are greatly appreciated. This work has been supported in part by the U.S. Department of Energy (DOE), Office of Basic Energy Sciences (Grant No. DE-FG02-93ER14331). Govind thanks Department of Science & Technology, Govt. of India, New Delhi, India.

[1] G. Ertl, H. Knözinger, F. Schüth, and J. Weitkamp, *Handbook of Heterogeneous Catalysis* (Wiley, New York, 1997).
[2] Q. Chen and N. V. Richardson, Prog. Surf. Sci. **73**, 59 (2003).
[3] R. E. Kirby, C. S. McKee, and M. W. Roberts, Surf. Sci. **55**, 725 (1976).
[4] R. E. Kirby, C. S. McKee, and L. V. Renny, Surf. Sci. **97**, 457 (1980).
[5] M. Sander, R. Imbihl, R. Schuster, J. V. Barth, and G. Ertl, Surf. Sci. **271**, 159 (1992).
[6] K. J. Song, J. C. Lin, M. Y. Lai, and Y. L. Wang, Surf. Sci. **327**, 17 (1995).
[7] A. T. S. Wee, J. S. Foord, R. G. Egdell, and J. B. Pethica, Phys. Rev. B **58**, R7548 (1998).
[8] T. E. Madey, C.-H. Nien, K. Pelhos, J. J. Kolodziej, I. M. Abdelrehim, and H.-S. Tao, Surf. Sci. **438**, 191 (1999).
[9] K. Pelhos, J. B. Hannon, G. L. Kellogg, and T. E. Madey, Surf. Sci. **432**, 115 (1999).
[10] D. B. Dańko, M. Kuchowicz, and J. Kolaczkiewicz, Surf. Sci. **552**, 111 (2004).
[11] I. Ermanoski, K. Pelhos, W. Chen, J. S. Quinton, and T. E. Madey, Surf. Sci. **549**, 1 (2004).
[12] H. Wang, W. Chen, and T. E. Madey, Phys. Rev. B **74**, 205426 (2006).
[13] J. Gustafson, A. Resta, A. Mikkelsen, R. Westerström, J. N. Andersen, E. Lundgren, J. Weissenrieder, M. Schmid, P. Varga, N. Kasper, X. Torrelles, S. Ferrer, F. Mittendorfer, and G. Kresse, Phys. Rev. B **74**, 035401 (2006).
[14] H. Wang, A. S. Y. Chan, W. Chen, P. Kaghazchi, T. Jacob, and T. E. Madey, ACS Nano **1**, 449 (2007).
[15] H. Wang, Ph.D. dissertation, Rutgers University, 2008; T. E. Madey, W. Chen, H. Wang, P. Kaghazchi, and T. Jacob, Chem. Soc. Rev. **37**, 2310 (2008).
[16] R. A. Campbell, J. Guan, and T. E. Madey, Catal. Lett. **27**, 273 (1994).
[17] R. Barnes, I. M. Abdelrehim, and T. E. Madey, Top. Catal. **14**, 53 (2000).
[18] W. Chen, I. Ermanoski, and T. E. Madey, J. Am. Chem. Soc. **127**, 5014 (2005).
[19] W. Chen, I. Ermanoski, T. Jacob, and T. E. Madey, Langmuir **22**, 3166 (2006).
[20] W. Chen, T. E. Madey, A. L. Stottlemyer, J. G. Chen, P. Kaghazchi, and T. Jacob, J. Phys. Chem. C **112**, 19113 (2008); W. Chen, A. L. Stottlemyer, J. G. Chen, P. Kaghazchi, T. Jacob, T. E. Madey, and R. A. Bartynski, Surf. Sci. **603**, 3136 (2009).
[21] M. Reyhan, H. Wang, and T. E. Madey, Catal. Lett. **129**, 46 (2009).
[22] M. Hansen and F. A. Shunk, *Constitution of Binary Alloys* (McGraw-Hill, New York, 1969).
[23] I. Ermanoski, Ph.D., Rutgers University, 2005.
[24] C. Z. Dong, S. M. Shivaprasad, K.-J. Song, and T. E. Madey, J. Chem. Phys. **99**, 9172 (1993).
[25] M.-C. Desjonqueres and D. Spanjaard, *Concepts in Surface Physics* (Springer-Verlag, Berlin, 1993).
[26] I. Ermanoski, C. Kim, S. P. Kelty, and T. E. Madey, Surf. Sci. **596**, 89 (2005).
[27] J. F. Nicholas, *An Atlas of Models of Crystal Surfaces* (Gordon and Breach, New York, 1965).
[28] P. W. Murray, F. M. Leibsle, Y. Li, Q. Guo, M. Bowker, G. Thornton, V. R. Dhanak, K. C. Prince, and R. Rosei, Phys. Rev. B **47**, 12976 (1993).
[29] F. M. Leibsle, P. W. Murray, S. M. Francis, G. Thornton, and M. Bowker, Nature (London) **363**, 706 (1993).
[30] C. Comicioli, V. R. Dhanak, G. Comelli, C. Astaldi, K. C. Prince, R. Rosei, A. Atrei, and E. Zanazzi, Chem. Phys. Lett. **214**, 438 (1993).
[31] C. Herring, Phys. Rev. **82**, 87 (1951).
[32] E. D. Williams and N. C. Bartelt, Science **251**, 393 (1991).
[33] L. Vitos, A. V. Ruban, H. L. Skriver, and J. Kollárb, Surf. Sci. **411**, 186 (1998).
[34] M. J. S. Spencer, A. Hung, I. K. Snook, and I. Yarovsky, Surf. Sci. **513**, 389 (2002).
[35] D. Yu and M. Scheffler, Phys. Rev. B **70**, 155417 (2004).
[36] H. P. Bonzel and M. Nowicki, Phys. Rev. B **70**, 245430 (2004).
[37] S. K. Kwon, Z. Nabi, K. Kádas, L. Vitos, J. Kollár, B. Johansson, and R. Ahuja, Phys. Rev. B **72**, 235423 (2005).
[38] C. W. Tucker, Jr., Acta Metall. **15**, 1465 (1967).

[39] D. A. Walko and I. K. Robinson, Phys. Rev. B **64**, 045412 (2001).
[40] S. H. Overbury, P. A. Bertrand, and G. A. Somorjai, Chem. Rev. **75**, 547 (1975).
[41] V. R. Dhanak, A. Baraldi, R. Rosei, M. Kiskinova, P. W. Murray, G. Thornton, and M. Bowker, Phys. Rev. B **50**, 8807 (1994).
[42] G. Comelli, V. R. Dhanak, M. Kiskinova, K. C. Prince, and R. Rosei, Surf. Sci. Rep. **32**, 165 (1998).
[43] J. D. Batteas, A. Barbieri, E. K. Starkey, M. A. V. Hove, and G. A. Somorjaia, Surf. Sci. **339**, 142 (1995).
[44] T. Hashizume, M. Taniguchi, K. Motai, H. Lu, K. Tanaka, and T. Sakurai, Jpn. J. Appl. Phys. **30**, L1529 (1991).
[45] K. Baberschke, U. Döbler, L. Wenzel, D. Arvanitis, A. Baratoff, and K. H. Rieder, Phys. Rev. B **33**, 5910 (1986).
[46] K. W. Jacobsen and J. K. Nørskov, Phys. Rev. Lett. **65**, 1788 (1990).
[47] J. Wintterlin, R. Schuster, D. J. Coulman, G. Ertl, and R. J. Behm, J. Vac. Sci. Technol. B **9**, 902 (1991).
[48] J.-W. He, U. Memmert, K. Griffiths, and P. R. Norton, J. Chem. Phys. **90**, 5082 (1989).
[49] P. van Beurden and G. J. Kramer, Phys. Rev. B **63**, 165106 (2001).
[50] J.-M. Zhang, H.-Y. Lia, and K.-W. Xub, J. Phys. Chem. Solids **67**, 1623 (2006).
[51] J.-M. Zhang, H.-Y. Li, and K.-W. Xu, Surf. Interface Anal. **39**, 660 (2007).
[52] K. Stokbro and S. Baroni, Surf. Sci. **370**, 166 (1997).